LETTER

Capillary interactions between nearby interfacial objects

View the article online for updates and enhancements.

You may also like

Recent citations

Capillary interactions between nearby interfacial objects

Andong He[(a)], Khoi Nguyen and Shreyas Mandre

Institute for Computational and Experimental Research in Mathematics, Brown University
Providence, RI 02912, USA

Abstract – We develop a general method to study the capillary interactions between objects of arbitrary shape which float close to each other on an interface, a regime in which multipole expansion is not useful. The force is represented as a power series in the small distance between the objects, of which the leading order is finite. For objects with size a much larger than the capillary length l_c, the force scales as $\sqrt{a/l_c}$ and the prefactor depends on the mean radius of curvature R at the closest points. After contact the objects roll and/or slide with respect to each other to locally maximize R and therefore the force. For smaller objects ($a \ll l_c$), the force scales as $(a/l_c)^{-1} \log(a/l_c)^{-2}$, and the prefactor depends only weakly on the shape and relative orientation of the objects.

Introduction. – Capillary interaction between objects on a fluid-fluid interface is an important mechanism for the pattern formation and stability of colloidal self-assembly [1–7], locomotion of meniscus-climbing insects [8–10], and seed dispersal of aquatic plants [11]. Depending on the objects and fluids, the force between the objects may be attractive or repulsive [12,13]. Previous studies have focused almost exclusively on the case when particles are far away from each other, either on an initially flat [14,15] or curved interface [16,17]. Within this framework a method based on multipole expansion assuming an undulating contact line has been widely adopted [18,19], and the interface deformation is treated as a linear superposition of the deformation due to individual particles [20–22]. However, when the density of the particles is high or as the particles self-assemble they come very close to each other, so the terms in the multipole expansion lose asymptotic ordering and the linear superposition ansatz becomes less useful.

In this paper, we develop a systematic method to calculate the horizontal capillary force between *nearby* interfacial objects and characterize its dependence on the shape and size of the objects assuming small interface deformation. The process of determining the force can be decomposed into two steps: the first is determining the meniscus shape for an object of three-dimensional geometry and surface wettability using the vertical force and torque balance, and the second is calculating the force resulting from the meniscus shape. Since the first step has received much attention, here we focus on the second step and show that the horizontal force depends *only* on the location of the contact line and not on the object geometry or the interface deformation. Our goal is to derive asymptotic expressions for the horizontal force expanded in the small distance d between the objects. We guide this derivation using numerical computations of the surface deformation, assuming without loss of generality the contact line to be pinned.

The asymptotic expansion of the force is found to be regular in d, but the coefficients of this expansion depend non-trivially on the characteristic horizontal size a of the objects. Two regimes in a emerge depending on their relation to the capillary length l_c, a scale over which the interface equilibrates to its unperturbed level. In the case $a \gg l_c$, the attractive capillary force is concentrated in the small region of closest approach between the objects. In the opposite regime $a \ll l_c$, we resort to a scaling analysis for the asymptotic form of the coefficients of the expansion, which depend weakly on the precise shape of the contact line. These coefficients and the range of validity of the asymptotic series are determined using

---

[(a)]Present address: Department of Geology and Geophysics, Yale University - New Haven, CT 06520-8109, USA.
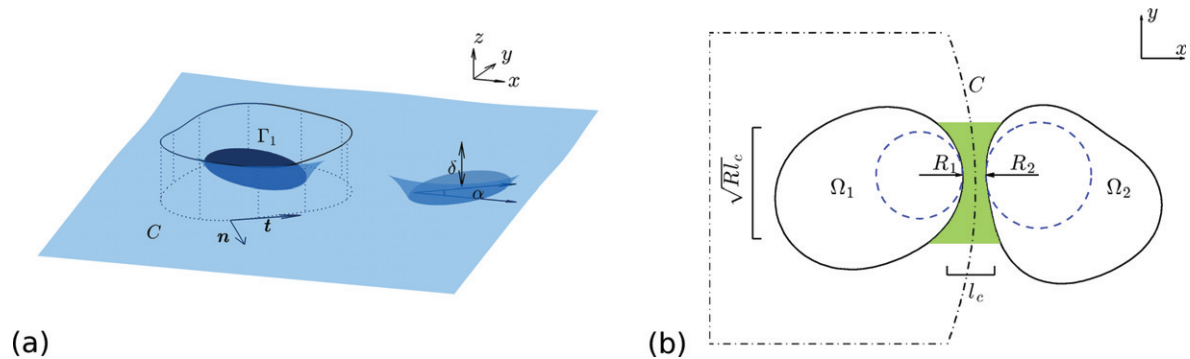
Fig. 1: (Color online) (a) The horizontal force between thin objects can be approximated by the line integral (2) on the base curve C. The object has a displacement δ at its center of mass, and a tilt angle α from the xy-plane. (b) Schematic showing the curve C (see text for its definition) in the xy-plane for two large neighboring objects. In this case the horizontal force is localized in the shaded region which has a characteristic length l_c and $\sqrt{Rl_c}$ in the x- and y-direction, respectively.

numerical computations, and are found to describe a wide range of object shapes. Finally, we compare our results to the case of objects that are far from each other.

Consider several objects on an interface between two fluids, with the contact line (either pinned or maintaining a contact angle) at the periphery Γ_i ($i = 1, 2, \ldots$), as schematically shown in fig. 1(a). The total force exerted on the i-th object is

$$\boldsymbol{F} = \sigma \int_{\Gamma_i} \dot{\mathbf{r}}(s) \times \boldsymbol{N}(s)\,\mathrm{d}s - \rho g \int_S u \boldsymbol{N}\,\mathrm{d}A, \qquad (1)$$

where σ is the surface tension, ρg the gravitational force density, $\dot{\mathbf{r}}(s)$ the unit tangent vector along Γ_i, $\boldsymbol{N}$ the unit normal to the surface pointing away from the liquid, u the surface displacement from the unperturbed level, $\mathrm{d}s$ the arclength differential, and $\mathrm{d}A$ the area element of the wetted surface S. The first and second integral in (1) represents the surface tension force and hydrostatic pressure force, respectively. This expression of the total force can be rewritten using force balance on an *arbitrary* control volume, formed by a vertical cylinder with a planar base curve C that encloses only one object and not others (fig. 1(a)). In hydrostatic equilibrium, the net force on the fluid portion in the control volume is zero. So (1) remains true if Γ_i is replaced by C and S by the surface of the control volume. As we shall demonstrate, choosing carefully a curve C leads us to a simple expression of the force.

The control volume argument leads naturally to a proof of the generalized Archimedes' principle for a single object [23], and an analogous Newton's third law for two arbitrary objects floating on an infinite surface [24]. The vertical component of (1) can be balanced by an externally applied force such as gravity or electromagnetic force and in the process determines the vertical displacement of the object. The horizontal component of $\boldsymbol{F}$ in (1) can be approximated to the leading order assuming $|\nabla u| \ll 1$ as

$$\boldsymbol{F}_h \approx \frac{\sigma}{2} \int_C \left[\left(\frac{u^2}{l_c^2} - u_n^2 + u_t^2 \right) \boldsymbol{n} - 2u_t u_n \boldsymbol{t} \right] \mathrm{d}t, \qquad (2)$$

where $l_c = \sqrt{\sigma/\rho g}$, $\boldsymbol{n}$ and $\boldsymbol{t}$ the unit normal and tangent vector to C respectively, $u_n = \nabla u \cdot \boldsymbol{n}$, $u_t = \nabla u \cdot \boldsymbol{t}$, and $\mathrm{d}t$ the arclength along C. Using (2) for calculating the horizontal force requires knowledge of u and its gradient, and (2) shows that in the small gradient limit the horizontal force scales with the square of the vertical displacement. A similar examination of the vertical force balance reveals that the vertical displacement is in turn proportional to the external vertical force.

The surface displacement u satisfies the linear free-surface equation [25–27]

$$u - l_c^2 \nabla^2 u = 0, \qquad (3)$$

which we solve numerically in the exterior of the objects using a boundary integral method [28]. Formally, a Dirichlet-Neumann map of the solutions to (3) provides u_n using u on the contact line, and use of (2) gives the horizontal force. This proves that knowledge of the contact line is sufficient for determining the horizontal force on the objects. To construct the map, we denote by $\boldsymbol{x}, \boldsymbol{\zeta}$ the position vectors; then u_n is given by

$$\mathrm{PV} \int_{\bigcup_i \Gamma_i} (u_n(\boldsymbol{x})G - u(\boldsymbol{x})\nabla_{\boldsymbol{x}}G \cdot \boldsymbol{n})\,\mathrm{d}s = \frac{u(\boldsymbol{\zeta})}{2l_c^2}, \qquad (4)$$

where $G = -\frac{1}{2\pi}K_0(|\boldsymbol{x} - \boldsymbol{\zeta}|/l_c)$ is the Green's function of (3), $K_0(|\boldsymbol{x}|)$ the modified Bessel function of the first kind [29], $\nabla_{\boldsymbol{x}}$ the gradient taken on $\boldsymbol{x}$, and "PV" the Cauchy principal value. A discretization of (4) and knowledge of u on Γ_i yields u_n numerically. In principle, (4) allows imposing $u = \delta_i(s)$ on the contact line Γ_i. However, different u on different objects leads to a large gradient of u because of the small distance between them, and in the limit $d \to 0$ requires a large (infinite in the small gradient formulation) vertical force and horizontal torque to maintain the vertical separation. A simple example of this divergence is seen explicitly for the horizontal force in our analysis for $a \gg l_c$ (*i.e.*, eq. (7)). Hence we anticipate u to be approximately equal on touching contact lines, and
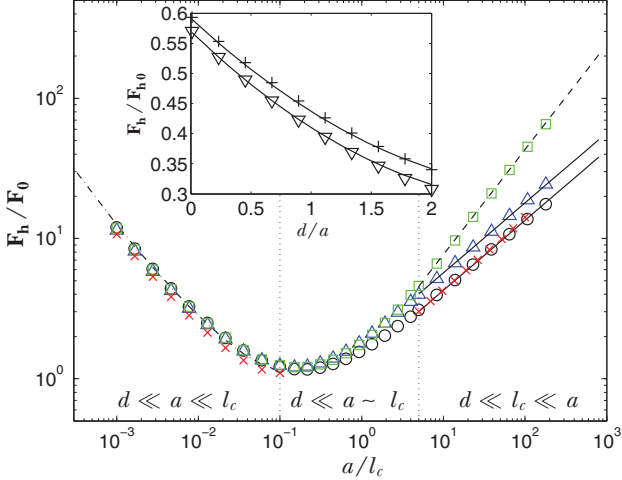
Fig. 2: (Color online) The dimensionless horizontal force $\boldsymbol{F}_h/\boldsymbol{F}_0$ (where $\boldsymbol{F}_0 = \sigma\delta^2/l_c$) for disks ($\circ$), side-by-side ellipses ($\triangle$) and superellipses of order 4 ($\square$) in the limit $d \to 0$. If $a \gg l_c$, the force scales as $\sqrt{a/l_c}$ for disks and ellipses (solid lines), and as $(a/l_c)^{1-1/k}$ for superellipses of order k (dashed line). If $a \ll l_c$, $\boldsymbol{F}_h \sim (a/l_c)^{-1}\log(a/l_c)^{-2}$ (dash-dotted line), with a prefactor depending weakly on the shape of the objects. The same scaling holds when the objects are allowed to tilt to satisfy torque balance ($\times$, for both large and small disks). Inset: the asymptotic expansion (8) for the rescaled force, with $\boldsymbol{F}_{h0} = \sigma\delta^2/a\log(a/l_c)^2$, shown as solid curves, is valid up to $d \approx 2a$ for small disks. Symbols are the numerically calculated values: $a/l_c = 10^{-4}$ ($\triangledown$), and 10^{-2} ($+$).

take $u = \delta_i(s) = \delta$ (constant) as the representative case to investigate the asymptotic form.

An object whose center displaces the surface by δ will generally tilt away from the xy-plane by an angle α (fig. 1(a)). For a given δ, α can be determined by a horizontal torque balance. Because the gravitational torque depends on the center of gravity, α may be different for objects of the same geometry, and so is the force of interaction. We choose to numerically impose $\alpha = 0$ or the center of gravity coinciding with the geometric centroid of the contact line as representative cases. From numerical solutions, we observe that the scaling for the horizontal force does not depend on α, although the prefactors have a weak dependence (fig. 2).

In fig. 2 the numerically calculated horizontal force between two disks, ellipses and superellipses of order k (shape given by $x^k + y^k = a^k$ for an even integer k) is shown as a function of the size of the objects. As $d \to 0$, $\boldsymbol{F}_h$ may be expanded as an asymptotic series, the leading term of which sets the scale of the horizontal force. The objects have only one length scale a (radius, major-axis, etc.). For large objects ($d \ll l_c \ll a$) we find that this leading-order force varies as $\sqrt{a/l_c}$ (except for the superellipses, which we describe separately), whereas for smaller objects ($d \ll a \ll l_c$) it varies as $(a/l_c)^{-1}\log(a/l_c)^{-2}$. The reason why different scaling laws arise with respect to a/l_c is that the interface equilibrates over a length scale l_c, as indicated by (3).

Objects much larger than the capillary length. – First, consider two nearby smooth objects Ω_1 and Ω_2 that are much larger than the capillary length ($d \ll l_c \ll a$) and deform the interface δ_1 and δ_2, respectively. We temporarily allow $\delta_1 \neq \delta_2$ to examine the effect of unequal displacements. The influence of the objects on each other is localized in the vicinity of the closest points (indicated by the shaded region in fig. 1(b)). Indeed, if u'_n denotes the surface gradient of Ω_1 as if Ω_2 is absent, then the difference $u_n - u'_n$ decays rapidly away from the small shaded region. Moreover, due to the slenderness of the shaded region we can simplify (3) using a lubrication-type approximation: $u_{yy} \ll u_{xx}$. Physically, this amounts to decomposing the meniscus into a series of one-dimensional capillary bridges between corresponding points on the periphery, calculating the force due to each individual bridge and summing to obtain the total force. The solution to (3) with this approximation is

$$u(x,y) = \frac{\delta_1 + \delta_2}{2} \frac{\cosh\left[(x - c(y))/l_c\right]}{\cosh\left[f(y)/2l_c\right]} - \frac{\delta_1 - \delta_2}{2} \frac{\sinh\left[(x - c(y))/l_c\right]}{\sinh\left[f(y)/2l_c\right]}, \quad (5)$$

where $f(y)$ is the distance between the peripheries of the objects at a given y, and $x = c(y)$ is the centerline of the gap, with the coordinate system chosen such that $c(0) = 0$, $f(0) = d$ and $c'(0) = f'(0) = 0$.

In order to simplify (2) we take a special curve C, composed of $x = c(y)$ and enclosing Ω_1 far away such that the contribution to the line integral (2) outside the shaded region is negligibly small. On this curve $u_t \ll u_n$, so the horizontal force from (2) and (5) reduces to

$$\boldsymbol{F}_h = \frac{\sigma}{8l_c^2} \int_{-\infty}^{\infty} \left[(\delta_1 + \delta_2)^2 \mathrm{sech}^2\left(\frac{f(y)}{2l_c}\right) \right.$$
$$\left. -(1 + c'(y)^2)(\delta_1 - \delta_2)^2 \mathrm{csch}^2\left(\frac{f(y)}{2l_c}\right) \right] \mathrm{d}y. \quad (6)$$

The first term in the integrand in (6) is attractive and the second term is repulsive. Near $y = 0$ we can expand $f(y) = d + b_2 y^2 + b_3 y^3 + \ldots$. For objects with finite radii of curvature R_1 and R_2 at the closest points, the dominant term in this expansion is generically $b_2 = 1/R \equiv (R_1 + R_2)/2R_1R_2$ which is the mean curvature. Note that (6) is valid for any δ_1 and δ_2 that may vary in y; if they are constant, the leading-order term of (6) simplifies to

$$\boldsymbol{F}_h \approx \frac{\Psi(2)\sigma(\delta_1 + \delta_2)^2}{8}\sqrt{\frac{R}{l_c^3}} - \frac{\pi\sigma(\delta_1 - \delta_2)^2}{4}\sqrt{\frac{R}{d^3}}, \quad (7)$$

with $\Psi(k) \equiv k^{1/k} \int_{-\infty}^{\infty} \mathrm{sech}^2(\eta^k)\,\mathrm{d}\eta$. The force is strongly repulsive at small d if $\delta_1 \neq \delta_2$, diverging as $d^{-3/2}$. Similar analysis shows that the vertical force and horizontal torque diverge as $1/d$. Assuming no agency applying such large forces and torques, as explained in the previous section, we limit our analysis to $\delta_1 = \delta_2 = \delta$.
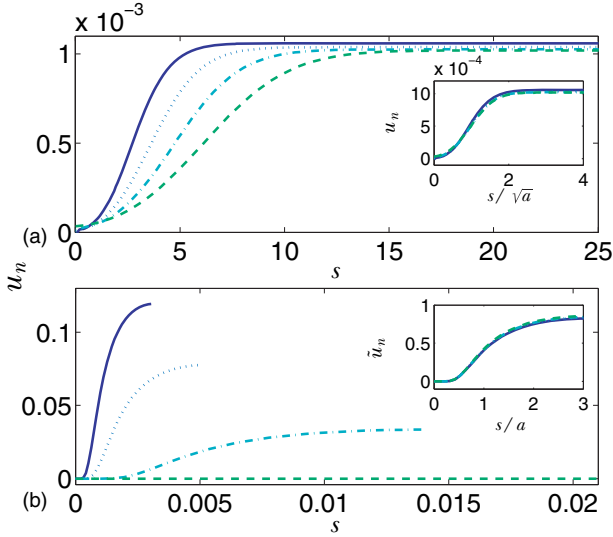
Fig. 3: (Color online) (a) The surface gradient u_n on the periphery of two disks approaches a constant value away from the shaded region (see fig. 1(b)) for large objects ($a/l_c = 8, 14, 23$ and 39 from the solid line to the dashed line); (b) u_n varies along the whole periphery for small ones ($a/l_c = 1.0 \times 10^{-3}, 1.7 \times 10^{-3}, 4.6 \times 10^{-3}$ and 1.0×10^{-1} from the solid line to the dashed line). The arclength $s = 0$ corresponds to the closest points. Insets: the collapse of the curves for different values of a (with $\tilde{u}_n = \frac{a \log(a/l_c) u_n}{\delta}$).

The first term in (7) is the product of the force per unit length of the capillary bridges scaling as $\sigma u_n^2 \sim \sigma \delta^2/l_c^2$, and the length scale $\sqrt{R l_c}$ in y over which this force is distributed. This scaling is shown in fig. 3(a) for disks of various radii a, in which case $R = a/2$. The curves for u_n computed using (4) collapse as a function of the arclength scaled by $\sqrt{a}$.

Because R is the mean radius of curvature at the closest points, two side-by-side ellipses experience a larger attractive force than two tip-to-tip ones do. We have also observed numerically that the force described in (7) in the asymptotic limit $d \ll l_c$ is valid up to $d \approx 5 l_c$, beyond the strict asymptotic criterion.

When $d = 0$, the objects are in contact, and any unbalanced torque causes them to rotate. They slide and/or roll along each other depending on the contact friction between them. We propose a mechanism for this relative motion as follows. The torque acting to rotate Ω_1 in the horizontal plane is given by $\tau \approx (\sigma \delta^2/2 l_c^2) \int_{-\infty}^{\infty} y \operatorname{sech}^2 (f(y)/2 l_c) \, \mathrm{d}s$. The leading-order contribution to τ is from the first non-zero odd power in the expansion of $f(y)$, which will generically be $b_3 y^3$. The effect of this net torque is to *increase* R as reflected by the sign of b_3: Ω_1 will rotate clockwise (counter-clockwise) if $b_3 < 0$ (> 0). The rotating torque is zero when $b_3 \approx 0$, corresponding to a maximum R. Thus, the equilibrium orientation of objects in contact is determined by maximizing R and consequently the force of interaction, subject to rolling or sliding constraints.
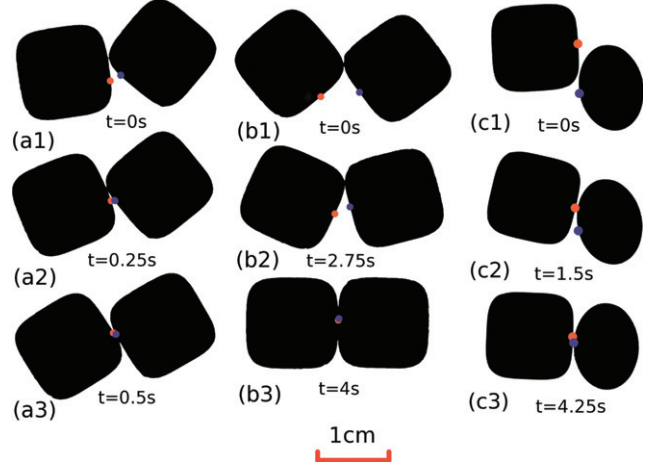

Fig. 4: (Color online) Two superellipses of order 4 with rough periphery starting with asymmetric (a1)–(a3) and symmetric (b1)–(b3) configuration roll along each other after contact, while one superellipse and one ellipse with smooth periphery can slide freely (c1)–(c3). The motion is such that the mean radius of curvature R at the contact point is maximized (predictions are shown by colored dots).

This proposal is supported by the experiments focusing on the rotation of two thin large objects in contact. Objects with various shapes are laser-cut from a $0.16 \, \mathrm{cm}$ thick acrylic sheet. Two such objects are gently released on the water surface in a $30 \, \mathrm{cm} \times 30 \, \mathrm{cm}$ tank and the subsequent motion is recorded at 4 frames per second using a Nikon D90 digital SLR camera. The tank is illuminated from below by a bright source (an Artograph LED light pad), and the camera is mounted vertically above the tank. The exposure is adjusted so that the background is saturated and the objects appear completely dark. As expected, the objects move towards each other due to capillary attraction. We observe two modes of motion after they contact depending on the friction between them: rolling and sliding. For objects with rough periphery the sliding motion is prohibited and thus the equilibrium orientation depends on the initial point of contact (asymmetric in fig. 4(a) and symmetric in (b)); but objects with smooth periphery can slide freely (fig. 4(c)). We compare the observations with the predicted equilibrium point of contact and find very good agreements in all cases.

The above symmetric configuration of the superellipses corresponds to a special and important case: R is infinite (so $b_2 = 0$) at the contact point. For such objects with isolated points of infinite R, the capillary interaction seeks these points and brings them in contact if the objects can slide freely. In this case $b_2 = 0$ and the force is proportional to the lowest non-zero even coefficient b_k. In particular, the force between two side-by-side superellipses of order k (as in fig. 4(b3)) is $\Psi(k)(\sigma \delta^2/2 l_c)(a/l_c)^{1-1/k}$. The dependence of this force on the size a is therefore stronger for larger k but always between $a^{1/2}$ and a for

Table 1: The size-independent coefficients λ_{ij} in $\boldsymbol{F}_h$ for small disks, ellipses with aspect ratio 4/3 and superellipses of order 4 (see eq. (8)).

Shape λ_{ij}	λ_{00}	λ_{01}	λ_{10}	λ_{11}	λ_{20}	λ_{21}
Disks	0.519	-0.389	-0.106	-0.075	0.010	0.014
Ellipses	0.483	-0.402	-0.091	-0.066	0.008	0.012
Superellipses	0.474	-0.612	-0.090	-0.007	0.007	0.004

smooth objects (fig. 2). In the limit $k \to \infty$, $\Psi(k) \to 2$, the objects resemble two squares, and $\boldsymbol{F}_h$ is proportional to a, which is the force between two large squares of side a estimated using a one-dimensional theory.

Objects much smaller than the capillary length. – For nearby objects that are much smaller than the capillary length ($d \ll a \ll l_c$), we invoke a different scaling argument motivated by matched asymptotic expansions. The outer solution (far away from the objects) behaves as $AK_0(r/l_c)$ for a suitable constant A, because the small objects appear as a point force when observed from length scale l_c. As $r \to a$, the outer solution must be matched with the inner solution which satisfies the boundary condition $u = O(\delta)$. Asymptotic matching on an intermediate length scale requires that the magnitude of outer solution on the inner length scale be comparable to the magnitude of inner solution, *i.e.* $AK_0(a/l_c) \propto \delta$, which determines A. The slope of the meniscus then scales as $u_n \propto -\delta K_1(a/l_c)/l_c K_0(a/l_c)$ which asymptotes to $\delta/a \log(a/l_c)$ as $a/l_c \to 0$. This scaling is verified in fig. 3(b), where we plot the surface gradient u_n for different radii. The curves collapse over two orders of magnitude in a. Substituting this scaling for u_n into (2) we get $\boldsymbol{F}_h \sim \sigma\delta^2/a \log(a/l_c)^2$. In fact, we can construct a double series for $\boldsymbol{F}_h$ in d/a and $\log(a/l_c)$ as

$$\boldsymbol{F}_h = \frac{\sigma\delta^2}{a} \sum_{i=0}^{\infty} \sum_{j=0}^{\infty} \lambda_{ij} \left(\frac{d}{a}\right)^i (\log(a/l_c))^{-(2+j)}, \quad (8)$$

where λ_{ij} are constants depending only on the geometric shape but not the size of the objects. The values of λ_{ij} are obtained by fitting to numerical data and given in table 1. The expansion in $\log(a/l_c)$ arises because of the asymptotic matching [30], similar to the problem of a low-Reynolds-number flow passing around a sphere or cylinder at higher orders in the Reynolds number [31,32]. Our simulations show that the asymptotic force described in (8) for $d \ll a$ is valid up to $d \approx 2a$ (inset of fig. 2), which we believe is due to the fast convergence of λ_{ij}.

Long-distance interactions. – In order to make connections with the long-distance interactions studied extensively in the literature [3,4,16,19,26], we extend our theory to far-apart objects ($a \ll d$). Using method of images, we can write the solution to (3) as a multipole
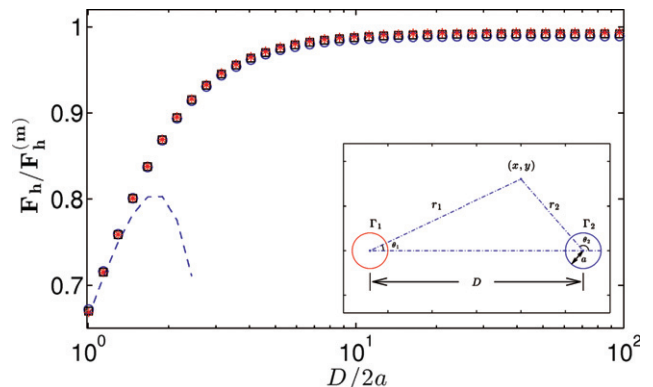

Fig. 5: (Color online) The horizontal force for the long- and short-distance case can be represented by a single curve, where $\boldsymbol{F}_h^{(m)}$ is given by (10); the dashed curve represents (8). Symbols are numerical results: $a/l_c = 10^{-10}, 10^{-8}$, and 10^{-6} for stars, squares, and circles, respectively. Inset: sketch of long-distance interaction between two disks with radius a and center-to-center distance D.

expansion:

$$u(x,y) = \sum_{n=0}^{\infty} A_n \left[K_n(r_1/l_c) \cos(n\theta_1) + (-1)^n K_n(r_2/l_c) \cos(n\theta_2) \right], \quad (9)$$

where K_n is the n-th order modified Bessel function of the first kind [29], and r_1, r_2, θ_1 and θ_2 are defined in fig. 5 inset. The coefficients A_n are determined by the boundary conditions on the periphery of the objects, which we take to be $u = \delta$ on Γ_1 and Γ_2. The first two coefficients are $A_0 = \delta/[K_0(a/l_c) + K_0(D/l_c)]$ and $A_1 = -a\delta K_1(D/l_c)/l_c K_1(a/l_c)[K_0(a/l_c) + K_0(D/l_c)]$ where $D = d + 2a$ is the distance between two centers. Note that in this long-distance limit A_0 and A_1 can be approximated by $\delta/K_0(a/l_c)$ and $-a\delta K_1(D/l_c)/l_c K_1(a/l_c) K_0(a/l_c)$, respectively. The leading-order horizontal force can be calculated as

$$\boldsymbol{F}_h^{(m)} = \frac{\pi a\sigma\delta^2 K_1(D/l_c)[aK_0(a/l_c) + 2l_c K_1(a/l_c)]}{l_c^3 [K_0(a/l_c) + K_0(D/l_c)]^2}. \quad (10)$$

The expression for $\boldsymbol{F}_h^{(m)}$ asymptotes to a power law in D when $D \ll l_c$, which recovers the result assuming superposition of the displacements [3], and exhibits an exponential decay in D when $D \gg l_c$.

The expression (10) is expected to be valid only for $D \gg a$ and inadequately describes the physics when $D \approx 2a$. This inaccuracy is confirmed by the numerical computations, as shown in fig. 5, where we plot the attractive force scaled by $\boldsymbol{F}_h^{(m)}$ as a function of $D/2a$ for values of a varying by 4 orders of magnitude. The rescaling collapses the force on a single universal curve. As expected, the force approaches the behavior described by (10) for $D/2a \gg 1$, but disagrees with the behavior for $D/2a = O(1)$. The latter regime is described accurately by (8).

Conclusion. – We develop a theory to study the dependence of the horizontal capillary force between nearby objects on their shape, size, and vertical displacements from the undeformed interface. The size of the objects relative to the capillary length governs the nature of their interaction: for large objects the force is crucially determined by their shapes via the mean radius of curvature at the closest points; for small objects the force is not localized in the vicinity of the closest points, and we derive a different scaling law based on matched asymptotic expansions. In both cases, we obtain analytical expressions of the force, which also reveal how the force depends on the distance between the objects. The numerical simulations show that these expressions are valid even beyond the strict validity of the asymptotic limits, and thus provide a convenient way to estimate the force. We also elucidate the mechanism for rotation of touching large objects from a geometric point of view, potentially useful for self-assembly of non-axisymmetric objects [1,4,16,33]. Our experiments using not-too-thin objects show excellent agreements with the theoretical predictions, so we believe that the consideration of thin objects is a useful approximation to study the capillary interactions of arbitrary 3D objects. Due to the relevance of capillary forces to a broad range of fields, and the simplicity and generality of our results, we expect wide applicability of these ideas in the scientific and engineering community.

$$* * *$$

REFERENCES

[1] Bowden N., Terfort A., Carbeck J. and Whitesides G., *Science*, **276** (1997) 233.
[2] Brown A. B. D., Smith C. G. and Rennie A. R., *Phys. Rev. E*, **62** (2000) 951.
[3] Kralchevsky P. A. and Nagayama K., *Adv. Colloid Interface Sci.*, **85** (2000) 145.
[4] Loudet J. C., Alsayed A. M., Zhang J. and Yodh A. G., *Phys. Rev. Lett.*, **92** (2005) 018301.
[5] Pergamenshchik V., *Phys. Rev. E*, **85** (2012) 021403.
[6] Vella D., Kim H. and Mahadevan L., *J. Fluid Mech.*, **502** (2004) 89.
[7] Vella D., Metcalfe P. and Whittaker R., *J. Fluid Mech.*, **549** (2006) 215.
[8] Bush J. W. M. and Hu D. L., *Annu. Rev. Fluid Mech.*, **38** (2006) 339.
[9] Hu D. L. and Bush J. W. M., *Nature*, **437** (2005) 733.
[10] Yu Y., Guo M., Li X. and Zheng Q. S., *Langmuir*, **23** (2007) 10546.
[11] Peruzzo P., Defina A. and Nepf H., *Water Resour. Res.*, **48** (2012) W07512.
[12] Mansfield E. H., Sepangi H. R. and Eastwood E. A., *Philos. Trans. R. Soc. London, Ser. A*, **355** (1997) 869.
[13] Vella D. and Mahadevan L., *Am. J. Phys.*, **73** (2005) 817.
[14] Bresme F. and Oettel M., *J. Phys.: Condens. Matter*, **19** (2007) 413101.
[15] Kalinin Y., Berejnov V. and Thorne R., *Langmuir*, **25** (2009) 5391.
[16] Cavallaro M., Botto L., Lewandowski E. P., Wang M. and Stebe K. J., *Proc. Natl. Acad. Sci. U.S.A.*, **108** (2011) 20923.
[17] Zeng C., Brau F., Davidovitch B. and Dinsmore A., *Soft Matter*, **8** (2012) 8582.
[18] Fournier J. B. and Galatola P., *Phys. Rev. E*, **65** (2002) 031601.
[19] Stamou D., Duschl C. and Johannsmann D., *Phys. Rev. E*, **62** (2000) 5263.
[20] Allain C. and Cloitre M., *J. Colloid Interface Sci.*, **157** (1993) 261.
[21] Chan D. Y. C., Henry J. J. D. and White L. R., *J. Colloid Interface Sci.*, **79** (1981) 410.
[22] Nicolson M. M., *Proc. Cambridge Philos. Soc.*, **45** (1949) 288.
[23] Keller J., *Phys. Fluids*, **10** (1998) 3009.
[24] Kralchevsky P. A. and Nagayama K., *Langmuir*, **10** (1994) 23.
[25] Cooray H., Cicuta P. and Vella D., *J. Phys.: Condens. Matter*, **24** (2012) 284104.
[26] Kralchevsky P. A., Paunov V. N., Ivanov I. B. and Nagayama K., *J. Colloid Interface Sci.*, **151** (1992) 79.
[27] Singh P. and Joseph D. D., *J. Fluid Mech.*, **530** (2005) 31.
[28] Pozrikidis C., *A Practical Guide to Boundary-Element Methods with the Software Library BEMLIB* (Taylor & Francis/CRC Press) 2002.
[29] Abramowitz M. and Stegun I. A., *Handbook of Mathematical Functions* (Dover, New York) 1965.
[30] Lo L., *J. Fluid Mech.*, **132** (1983) 65.
[31] Veysey J. and Goldenfeld N., *Rev. Mod. Phys.*, **79** (2007) 883.
[32] Hinch E. J., *Perturbation Methods* (Cambridge University Press) 1991.
[33] van Nierop E. A., Stijnman M. A. and Hilgenfeldt S., *Europhys. Lett.*, **72** (2005) 671.